

# Mitigating Heterogeneity in Federated Multimodal Learning with Biomedical Vision-Language Pre-training

Zitao Shuai<sup>1</sup> Liyue Shen<sup>1</sup>

## Abstract

Vision-language pre-training (VLP) has arisen as an efficient scheme for multimodal representation learning, but it requires large-scale multimodal data for pre-training, making it an obstacle especially for biomedical applications. To overcome the data limitation, federated learning (FL) can be a promising strategy to scale up the dataset for biomedical VLP while protecting data privacy. However, client data are often heterogeneous in real-world scenarios, and we observe that local training on heterogeneous client data would distort the multimodal representation learning and lead to biased cross-modal alignment. To address this challenge, we propose **Federated distributional Robust Guidance-Based (FedRGB)** learning framework for federated VLP with robustness to data heterogeneity. Specifically, we utilize a *guidance-based local training* scheme to reduce feature distortions, and employ a *distribution-based min-max optimization* to learn unbiased cross-modal alignment. The experiments on real-world datasets show our method successfully promotes efficient federated multimodal learning for biomedical VLP with data heterogeneity.

## 1. Introduction

Vision-language pre-training (VLP) learns efficient multimodal representations by extracting latent semantics from a large amount of image-text pairs, where the dataset scale largely impacts the performance of the learned model (Oquab et al., 2023). However, enlarging pre-training dataset is a non-trivial challenge especially for biomedical applications which is restricted by privacy issues of clinical and patient data (Ladbury et al., 2023). To utilize data across different institutes, recent work (Lu et al., 2023a) has attempted to introduce federated learning into the biomedical VLP domain.

<sup>1</sup>EECS Department, University of Michigan. Correspondence to: Liyue Shen [liyues@umich.edu](mailto:liyues@umich.edu).

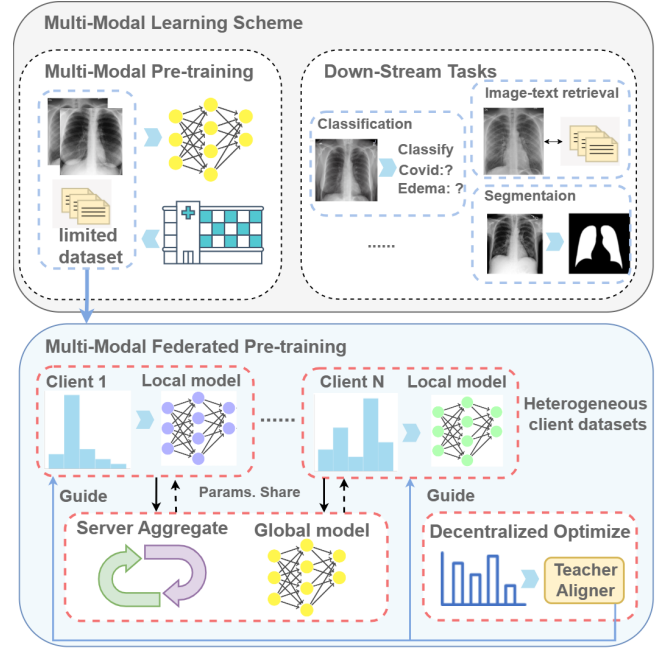


Figure 1. Federated multi-modal pre-training aims to decentralizedly utilizing private dataset to tackle the data hungry problem. Fitting heterogeneous local datasets that correspond to different distributions of latent semantics (e.g. disease) would result in biased models. Our FedRGB framework has successfully upgraded multi-modal pretraining methods by introducing robust alignment module as guidance during local training time.

However, in real-world scenarios, datasets collected from different institutes are always heterogeneous, which is a long-standing practical challenge in federated learning (Ghosh et al., 2019; Zhang et al., 2023a; Huang et al., 2022). For example, one hospital receives a high proportion of patients with pneumonia, while another hospital may undertake more patients with tuberculosis, due to variety of patients cohort and geographics. While the data heterogeneity would essentially damage the performance of the federally trained model, current FL methods for biomedical VLP (Lu et al., 2023a) haven’t taken this vital factor into consideration to provide an effective solution.

To address this issue, simply averaging client models trained on heterogeneous local datasets results in biases as shown in Figure 1. Firstly, the client model would be heterogeneous, and re-training on the sent-back server model might

distort the aggregated structure of the representation space. Secondly, averaging model parameters cannot produce a robust alignment between the two modalities, which not only affects the generalization ability, but also prevents the model from learning more diverse correlations between vision and language. Furthermore, as we will demonstrate in our empirical findings (Sec 5.2), heterogeneity harms the performance of pre-trained model by affecting the deep layers which serve as an alignment module in the VLP model.

In this paper, we propose the FedRGB framework to mitigate heterogeneity in federated biomedical VLP to enable its deployment in real-world scenarios. To alleviate the distortion in local client training, we introduce a teacher alignment module to provide unbiased cross-modal alignment by generating anchor representation space for regularization. We employ a distributionally robust optimization (DRO)-based algorithm to learn a robust teacher alignment module, which is optimized to better alleviate the worst-case distortion on the feature encoder caused by local cross-modal alignment.

Our contributions primarily focus on:

- We for the first time tackle the problem of biomedical VLP under the federated setting by utilizing heterogeneous datasets from different institutes. We conduct empirical studies to analyze the influence of data heterogeneity on federated multimodal learning.
- We propose FedRGB framework to mitigate the heterogeneity in federated multimodal learning. Specifically, our method introduces the guidance-based local training scheme for learning unbiased cross-modal alignment to alleviate representaiton distortions.
- Experiment results show the effectiveness of our method in learning multimodal representations under the federated setting by appling to various downstream tasks including image-text retrieval, classification, and segmentation.

## 2. Related Work

### 2.1. Vision-Language Pre-training

**Vision-Language Pre-training (VLP):** Leveraging data of different modalities to enable multimodal reasoning and representation learning for various cross-modal tasks has become an active research field in machine learning (Radford et al., 2021). Pre-training vision-language models on large datasets and then transferring learned knowledge to downstream tasks has become a popular approach to extract semantics from unlabeled image-text paired datasets (Li et al., 2022a; Bao et al., 2022). To find the shared latent space, current works often focus on learning generalizable and robust alignment relationships between the two modalities

(Radford et al., 2021; Chen et al., 2020a), which measures the ability to connect and retrieve the representation of the paired data.

**Biomedical Vision-Language Pre-training:** Most of the existing works in biomedical vision-language pre-training are based on the twin modality-specific encoders for medical images and reports respectively, with the image-report contrastive loss (Zhang et al., 2022b) to align visual and language representations on a joint latent space. A significant improvement has been achieved using the local contrastive loss which aims to align fine-grained representations (Huang et al., 2021). Incorporating medical domain knowledge, Wang et al. (2022) proposes a well-designed method that aligns the image and report embeddings in three different granularities. Recent works have also tried to address other practical issues of misalignments (Banur et al., 2023). However, most of these methods haven't considered the adaptation to de-centralized scenarios during pre-training and thus might fail to handle the potential damage from data heterogeneity.

### 2.2. Federated Learning

**Heterogeneous Federated Learning:** Federated learning aims to de-centralize model training by aggregating models trained on local clients to obtain more generalizable models with scaled-up training datasets while protecting data privacy (McMahan et al., 2017), which achieved success in many applications especially those with data privacy issues like biomedical data. However, client datasets are heterogeneous in most cases, which damages the performance of the aggregated model (Ghosh et al., 2019). Existing methods have tried to solve the data heterogeneity problem in many ways (Li & Wang, 2019; Collins et al., 2021). However, most methods either require additional communications on representations (Zhang et al., 2023a) which are not privacy-preserved and inefficient, or need large-scale public datasets for server aggregation (Huang et al., 2022; Yu et al., 2023b) that does not fit the case for biomedical data. Besides, remaining methods are often designed for supervised tasks that focus on label distribution (Diao et al., 2020) or feature distribution (Li et al., 2022b), which cannot be directly adapted to the vision-language pre-training task. While the self-supervised pre-trained models can be biased due to the heterogeneous datasets in the biomedical domain (Krishnan et al., 2022) and over-reliance on spurious features (Saab et al., 2022), distributionally robust optimization (Deng et al., 2020) can optimize the worst-case performance thus alleviating these issues (Liu et al., 2022). Recent works have considered its application in unsupervised and self-supervised learning scenarios (Han et al., 2023; Zhang et al., 2022a; Capitani et al., 2024).

**Federated Multi-modal Learning:** Federated learning

strategies have been extended to multimodal datasets in recent works (Zhou & Wang, 2022), with the goal to reduce training cost and promote personalized deployment of multimodal foundation models (Su et al., 2022; Chen et al., 2023b; Lu et al., 2023b). For example, Yu et al. (2023a) considers a client-server collaborative pre-training setting, benefiting the pre-training process of the server model by leveraging representations from local modalities. Nevertheless, these works require a pre-training stage in the server while ignoring that only on client datasets with limited samples. The closest work to ours is Lu et al. (2023a), which adopts federated learning to scale up the pre-training dataset. However, this work lacks generalization ability and hasn't considered the data heterogeneity issue that is very common and significant in practice.

### 3. Problem Formulation

We aim at mitigating the data heterogeneity issues in federally pre-training biomedical vision-language models to better capture the semantic alignment between the two modalities, with heterogeneous private datasets from different clients. In this section, we will formulate our problem setup and assumptions. Please see Appendix A for the detailed preliminary.

**Federated Vision-Language Pre-training.** In this paper, we consider the federated vision-language pre-training (VLP) problem in the biomedical domain. Suppose we are given  $N$  clients  $\{C_i\}_{i=1}^N$ , each client has a corresponding local yet private dataset  $\{D_i\}_{i=1}^N$  that can't be easily shared due to privacy issues. Without access to centralized pre-training, federated pre-training aims to conduct vision-language representation learning across local clients, while still capture a robust and generalizable cross-modal alignment, by efficiently aggregating client models  $\{M_i\}_{i=1}^N$  trained on their private datasets.

Similar to conventional federated learning scenarios, our federated pre-training consists of multiple communication turns. For communication turn  $t$ , client models  $\{M_i\}_{i=1}^N$  completed the same number of local iteration steps respectively, and the server receives and aggregates the weights sent from local models to produce the aggregated server model  $M^t$ . Then it will be sent back to clients and re-trained on  $\{D_i\}_{i=1}^N$  separately to get new local models  $\{M_i^{t+1}\}_{i=1}^N$ .

The federated vision-language pre-training is a more practical and general task compared to related works. Table 3 lists the most similar settings in previous works, and the difference between our task and theirs.

**Data Formulation.** We consider the multimodal datasets including vision and language modalities  $X, Y$ , consisting of respective data samples  $X = \{x_i\}_{i=1}^n, Y = \{y_i\}_{i=1}^m, n, m \in N^+$ . We assume there exists latent vari-

Table 1. Comparison between related multi-modal federated learning tasks and our federated biomedical vision-language pre-training task. We organize the related works according to our key areas of interest. (1). Heterogeneous clients. (2). Multi-modal clients. (3). Transferability. (4). Prior model-free. (5). No communication on public data or feature representations.

Task	hetero.	m.m.c.	transf.	no prior	no feat. com.
(Yu et al., 2023a)	✓		✓		
(Lu et al., 2023b)	✓	✓			✓
(Chen et al., 2023b)	✓	✓	✓		✓
(Lu et al., 2023a)		✓		✓	✓
FedRGB	✓	✓	✓	✓	✓

ables  $U$  that embed semantics across two modalities. For example, the disease category of a given X-ray radiology-report pair is a latent variable connecting these two modalities, which determines the pathology region of the radiology image and semantics in the diagnosis report. For heterogeneous local datasets, we assume the distribution of latent variables  $P_i(U)$  is different across clients.

### 4. Method

We propose a de-centralized framework to mitigate the data heterogeneity in federated biomedical vision-language pre-training, for learning an efficient vision-language model that can robustly capture reliable cross-modal semantic alignments. In this section, we first introduce our approach with a guidance-based local training strategy to reduce the distortion on encoders caused by fitting client datasets. Secondly, we will illustrate how our approach employ a distribution-based min-max optimization to learn unbiased cross-modal alignment. Algorithm 1 shows the pipeline of our method.

#### 4.1. Guidance-based Local Client Training

As shown in our empirical findings (Sec. 5.2), biomedical vision-language models pre-trained on heterogeneous client datasets are affected by the local correlations of the two modalities, which can't be addressed by simply averaging the weights of local models. Furthermore, this mainly falls on the deep layers which act as alignment modules, where the heterogeneous alignment module would distort the learned encoder during local iterations as shown in Sec. 5.2. Inspired by these findings, we introduce a teacher aligner to guide the representation space learned by local models to converge to a generalizable and robust one.

**Teacher alignment module.** To alleviate the distortion and bias when learning local features encoders and alignment modules, we propose to utilize a teacher alignment module to generate anchor representations conditioned on the output feature vector of the encoder to encourage local models to learn a homogeneous representation space

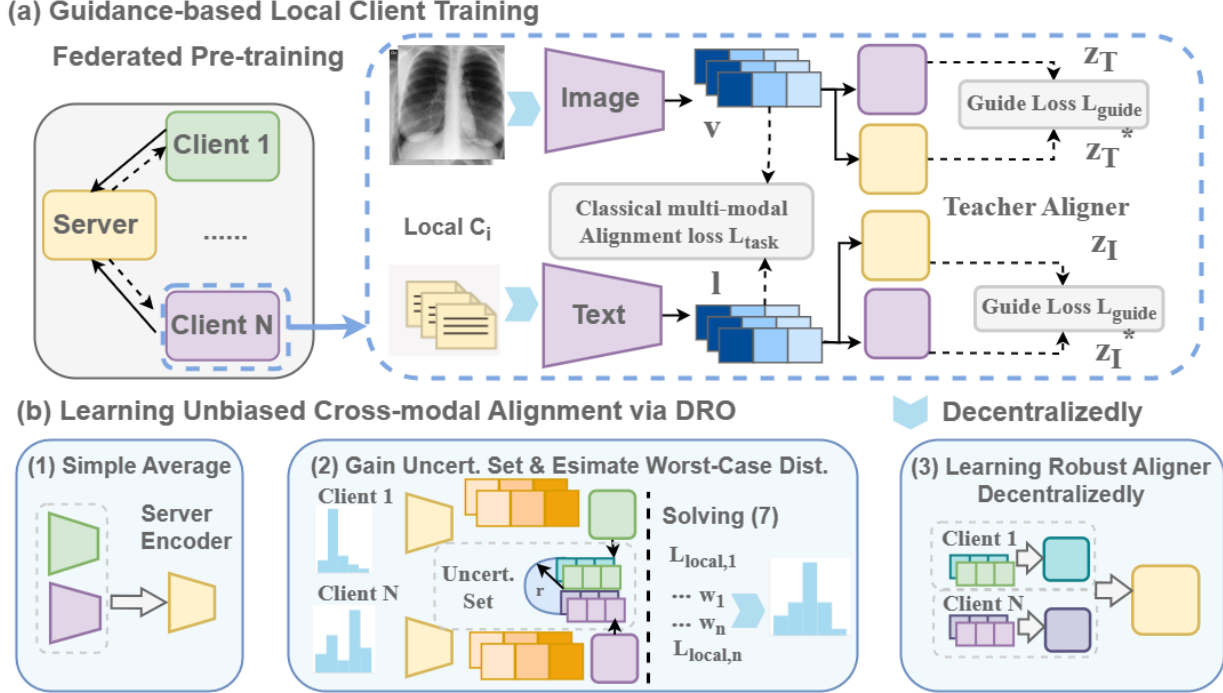


Figure 2. (a) Our proposed FedRGB upgrades backbone multi-modal pre-training strategies via introducing a robust guidance to local pre-training. This approach can reduce the distortion on feature encoders and learn better cross-modal alignment. (b) We employ a distribution-based min-max optimization to learn robust cross-modal alignment, which will be used as guidance in local pre-training.

across clients. Suppose after one client-server communication turn, given the local dataset of client  $c \in \mathcal{C}$  sampled from  $(x^c, y^c) \sim D_c$ , and teacher alignment module  $g_v^*, g_l^*$  corresponding to vision and language modality, we target at updating the feature encoders of image and text  $f_v, f_l$  and the corresponding alignment modules  $g_{img}, g_{txt}$ , by training on the local client dataset  $D_c$ , under the guidance of teacher alignment modules.

**Guiding local training with robust aligner.** As shown in Fig. 2, given the image-text pairs from local dataset as input  $(x^c, y^c) \sim D_c$ , we denote the feature vectors output from the feature encoder modules as  $(v^c, l^c)$ . Then getting through the alignment module, the aligned representations output from local aligners are denoted by  $(z_I^c, z_T^c)$ , while those from teacher aligners are  $(z_I^{c*}, z_T^{c*})$ . The goal is to reduce the discrepancy between two sets of aligned representations produced by local and teacher aligners, so that we can keep locally trained model will not be misled by the bias from local datasets and all local clients can converge to learn a similar embedding space that captures globally reliable and generalizable cross-domain alignment.

The teacher guidance loss can be formulated as below:

$$\mathcal{L}_{guide} = \sum_{i=1}^{N_c} (z_{I,i}^{c*} - z_{I,i}^c)^2 + \sum_{i=1}^{N_c} (z_{T,i}^{c*} - z_{T,i}^c)^2 \quad (1)$$

, where  $N_c$  refers to the number of samples in client the  $c$ .

We combine the guidance loss with the optimization goal  $\mathcal{L}_{task}$  of the initial biomedical vision-language pre-training method, which includes e.g. image-text contrastive loss in ConVIRT (Zhang et al., 2022b). The overall loss function for local client training can be written as:

$$\mathcal{L}_{local} = \mathcal{L}_{guide} + \alpha \mathcal{L}_{task} \quad (2)$$

where  $\alpha$  is the hyper-parameter that balances between guidance regularization and training task in local client updating.

## 4.2. Learning Unbiased Cross-modal Alignment via Distribution-based Optimization

In order to guide the local client training, we need to provide a teacher alignment module as mentioned in the last section, which can capture globally unbiased and generalizable cross-domain alignment. How can we obtain such a teacher guidance model? We propose to learn the unbiased cross-domain alignment by considering the robustness across various distributions of local clients. Detailed problem formulation and description could be seen in Appendix B.

A teacher alignment module should avoid distorting the aggregated feature encoder while learning the unbiased cross-modal alignments. Additionally, we introduce a much harder task to force the module to be more robust to biased alignment, by considering the influence of the biased alignment module on the feature encoder. Furthermore, to learn a teacher model that performs well on varies data distributions,



we minimize distortion degree under the most biased local alignment with the ‘‘worst-case’’ local data distribution.

**Learning robust cross-modal alignment through distributionally robust optimization.** Inspired by the distributionally robust optimization (DRO) (Cotter et al., 2019), we model the de-centralized pre-training framework as a two-stage DRO learning process. In the first stage, the local models are trained with  $\mathcal{L}_{local}$  (Eq. 2), while the whole model is jointly optimized with the guidance of the teacher alignment module. In the second stage, we employ the decentralized DRO approach to learn a robust teacher alignment module that performs well conditioned on the worst-case local models where the feature encoder is distorted the most severely.

**Learning object of alleviating distortion in local training.** After finishing the local training in each communication round, we aim to employ an extra de-centralized learning process in the client-side to optimize the alignment module on the worst-case distribution of an uncertainty set constructed by the local aligner and local data distribution, denoted as  $P_i$  for simplicity. The uncertainty set can be written as:

$$Q^c : \{D(Q||P^c) \leq \rho\}, P^c = \sum_{i=1}^N w_i P_i, w \in \Delta_{N-1} \quad (3)$$

where  $N$  is the number of clients,  $\Delta$  is a  $(N-1)$ -dim simplex,  $D$  is a discrepancy measure, and  $\rho$  is the uncertainty radius that measures the uncertainty degree of the unseen distributions and influences model’s generalization ability. The details of the  $P_i$  can be seen in Appendix B.

With the teacher alignment module denoted as  $g^*$  and the aggregated encoder  $f^*$  after the first stage training, the optimization goal can be constructed by distributions  $P_i$  of the support set:

$$\min_{g^*} \max_{\mathbf{w} \in \Delta_{N-1}} \sum_{i=1}^N w_i \mathcal{L}_{dro}(g^*, P_i, f^*), s.t. D(N\mathbf{w}||\mathbf{1}) \leq \rho \quad (4)$$

,where  $\mathcal{L}_{dro}(g^*, P_i, f^*)$  are the losses calculated on the local clients respectively. While we learn  $g^*$  by gradient descent, employing an alternative optimization approach, the mirror gradient descent process of optimizing  $\mathbf{w}$  could be solved efficiently (Zhang et al., 2023b; Duchi et al., 2008):

$$w_i^{(r+1)} = \text{Proj}_{\mathcal{Q}_c} \left( w_i^{(r)} e^{\gamma v_i^{(r)}} / \sum_{i=1}^N w_i^{(r)} e^{\gamma v_i^{(r)}}, \rho \right) \quad (5)$$

where  $\text{Proj}_{\mathcal{Q}_c}$  refers to the projection to  $\{w : D(N\mathbf{w}||\mathbf{1}) \leq \rho\}$ ,  $v_i$  represents the loss  $\mathcal{L}_{dro}(g^*, P_i, f^*)$ ,  $r$  refers to the communication turn.

Finally, we formulate  $\mathcal{L}_{dro}$  to measure the performance of the teacher alignment module of alleviating distortion on the encoder. Based on Eqs 3 and 4, we update the teacher

---

**Algorithm 1** Algorithm 1

**Require:** Clients  $N$ ; Communication rounds  $R$ ; learning rate  $\eta$ ; weight update stepsize  $\gamma$ ; encoder  $\Theta^{(0)}$ ; align module  $\theta^{(0)}$ ; robust align module  $\theta^{(0)*}$ ; client weight  $\{w_c^{(0)}\}$ ; uncertainty set radius  $\rho$ ; client datasets  $\{D_i\}_{i=1}^N$ ; Local iteration steps  $E$ .

- 1: **for**  $r = 0, \dots, R-1$  **do**
- 2: Server broadcasts  $\Theta^{(rE)}, \theta^{(rE)}, \theta^{(rE)*}, \{w_k^{(rE)}\}$
- 3: Compute loss  $v_c^{(r)}$  of model  $(\Theta_i^{(t)}; \theta_i^{(t)})$  on dataset  $D_c^i$
- 4: **for** client  $i = 1, \dots, N$  **do**
- 5: Set  $(\Theta_i^{(rE)}; \theta_i^{(rE)}; \theta_i^{(rE)*}) = (\Theta^{(rE)}; \theta^{(rE)}; \theta^{(rE)*})$
- 6: **for**  $t = rE, \dots, (r+1)E-1$  **do**
- 7: Sample  $\xi_i^{(t)}$  from  $D_i$  uniformly
- 8:  $(\Theta_i^{(t+1)}; \theta_i^{(t+1)}) = (\Theta_i^{(t)}; \theta_i^{(t)}) -$
- 9:  $\eta \nabla_{(\Theta_i; \theta_i)} \mathcal{L}_{local}((\Theta_i^{(t)}; \theta_i^{(t)}; \theta_i^{(rE)*}); \xi_i^{(t)})$
- 10: **end for**
- 11: The client sends  $\theta_i^{((r+1)E)}, v_c^{(r)}$  to the server
- 12: **end for**
- 13: Server computes:  $\Theta^{((r+1)E)} = \frac{1}{N} \sum_{i=1}^N \Theta_i^{((r+1)E)}$
- 14: **for** client  $i = 1, \dots, N$  **do**
- 15:  $w_c^{(r+1)} = \text{Proj}_{\mathcal{Q}_c} \left( w_c^{(r)} e^{\gamma v_c^{(r)}} / \sum_{i=1}^N w_c^{(r)} e^{\gamma v_c^{(r)}}, \rho \right)$
- 16: **end for**
- 17: **for** client  $i = 1, \dots, N$  **do**
- 18:  $(\Theta_i^{((r+1)E)}; \theta_i^{((r+1)E)}) = (\Theta^{((r+1)E)}; \theta^{((r+1)E)})$
- 19: Set  $\theta_i^{rE*} = \theta^{rE*}, \Theta_i^{rE*} = \Theta^{rE*}$
- 20: **for**  $t = rE, \dots, (r+1)E-1$  **do**
- 21: Sample  $\xi_i^{(t)}$  from  $D_i$  uniformly
- 22:  $(\theta_i^{(t+1)*}; \Theta_i^{(t+1)*}) = (\theta_i^{(t)*}; \Theta_i^{(t)*}) -$
- 23:  $w_c^{(r+1)} \eta \nabla_{\theta^*, \Theta} \mathcal{L}_{dro}(\Theta_i^{(t)}; \theta_i^{(t)}; \theta_i^{(rE)*}); \xi_i^{(t)*}; \xi_i^{(t)})$
- 24: **end for**
- 25: **end for**
- 26: Server computes:  $\theta^{((r+1)E)*} = \frac{1}{N} \sum_{i=1}^N \theta_i^{((r+1)E)*}$
- 27: Set parameters:  $\theta^{((r+1)E)} = \theta^{((r+1)E)*}$
- 28: **end for**

**Ensure:**  $(\Theta^{(RE)}; \theta^{(RE)})$

---

alignment module in local clients with weights  $\mathbf{w}$ . Specifically, given a client  $c$ , we use  $f^*$  learned in the first stage of the current communication turn to generate features  $(\tilde{v}^c, \tilde{l}^c)$  which are not distorted by the local aligner during the second stage’s training. And a learnable copy of  $f^*$  to generate distorted features  $(v^c, l^c)$ . The distorted features are input to the frozen local aligner  $g$  to calculate the task loss  $\mathcal{L}_{task}$ , and are also input to the teacher aligner  $g^*$  to get calibrated representations  $(z_I^{c*}, z_T^{c*})$ . Meanwhile,  $(\tilde{v}^c, \tilde{l}^c)$  are input to  $g^*$  to get representation  $(\tilde{z}_I^{c*}, \tilde{z}_T^{c*})$  as anchors for  $(z_I^{c*}, z_T^{c*})$  projected by teacher aligner using distorted features, for regularization. The learning object of the second stage could be written as:

$$\mathcal{L}_{dro} = \beta \left( \sum_{i=1}^{N_c} (z_{I,i}^{\tilde{c}*} - z_{I,i}^{c*})^2 + \sum_{i=1}^{N_c} (z_{T,i}^{\tilde{c}*} - z_{T,i}^{c*})^2 \right) + \mathcal{L}_{CL} + \mathcal{L}_{task} \quad (6)$$

,where  $\mathcal{L}_{CL}$  is the contrastive loss (Radford et al., 2021) between  $(z_I^{c*}, \tilde{z}_I^{c*})$ ,  $\mathcal{L}_{task}$  refers to the loss function of the backbone pre-training method and  $N_c$  refers to the number of samples in the client  $c$ .

## 5. Experiment

### 5.1. Experiment Setting

#### 5.1.1. PRE-TRAINING SETUP

Following (Wang et al., 2022), we utilize the MIMIC-CXR (Bigolin Lanfredi et al., 2022) dataset for biomedical vision-language pre-training. During the de-centralized pre-training process, local clients only have access to their private datasets. Following Yan et al. (2023), we employ the Latent Dirichlet Allocation (LDA) (Blei et al., 2003) to divide the MIMIC-CXR dataset based on a 5-way disease attribute to construct the heterogeneous client datasets. We set the heterogeneity degree in the LDA algorithm to be 1. The client datasets are highly heterogeneous as shown in Figure 3 and the appendix. We divide the MIMIC-CXR into 5 heterogeneous subgroups to construct 5 clients. Each divided dataset consists of train splits and validation splits based on the notation of the MIMIC-CXR. For the pre-training reported in the main table, we set the number of communications to 25, and we randomly sampled 50 batches of data from the client datasets for each communication. For more details, please see the appendix. For analysis experiments on out-of-distribution generalization ability, we utilize the EHRXQA (Bae et al., 2023) to evaluate the transferability of the pre-trained model to the unseen domain.

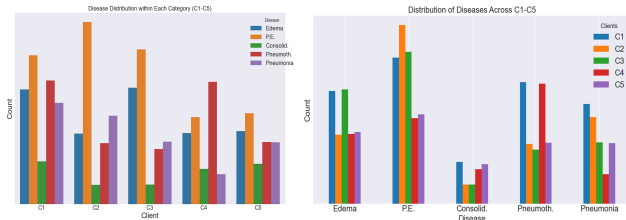


Figure 3. The descriptive statistic of the divided 5 subgroups, it can be seen that they are highly heterogeneous.

#### 5.1.2. DOWNSTREAM TASKS

We conduct several downstream tasks following (Wang et al., 2022) to evaluate the generalization ability of the pre-trained model. For more details, please see the appendix.

**Few-shot classification.** We test their performance on multiple image classification benchmarks: (1) RSNA Pneumonia Detection (RSNA) (Shih et al., 2019). (2) Covidx (Wang et al., 2020). We fine-tune our pre-trained model with an additional linear layer on 1%, 10% percentage of the training dataset, and evaluate the classification accuracy.

**Medical image segmentation.** We conduct experiments following (Wang et al., 2022) on medical image segmentation on the RSNA (Wang et al., 2020) benchmark. We freeze the encoder and fine-tune a U-Net decoder using 1%, 10% of the training data, and then use the Dice score for evaluation.

**Image retrieval.** To verify the pre-trained models have learned semantics and cross-modal alignments, we conduct the image retrieval task. Specifically, we utilize the validation splits of the clients for evaluation, these datasets are unseen in pre-training. We utilize the top-1 recall accuracy and top-5 recall accuracy to evaluate the pre-trained models.

#### 5.1.3. BACKBONES AND BASELINES

We focus on upgrading biomedical vision-language pre-training (VLP) strategies to heterogeneous federated learning scenes. Since federated heterogeneous VLP is a new topic, we adopt existing biomedical VLP baselines to federated strategies (Lu et al., 2023a). Specifically, we consider adopting simple language-image contrastive alignment (ConVIRT) (Zhang et al., 2022b; Radford et al., 2021), global-local language-image contrastive alignment (GLORIA) (Huang et al., 2021), and Multi-Granularity Cross-modal Alignment (MGCA) (Wang et al., 2022). Since the federated multi-modal pre-training is a novel setting, we adapted FedMAE (Yan et al., 2023), FedEMA (Zhuang et al., 2022), and FedX (Han et al., 2022) for comparison. These are self-supervised learning methods in the federated learning domain which also focus on tackling the data heterogeneity. For basic federated learning baselines, we consider simple averaging (FedAvg) (McMahan et al., 2017; Lu et al., 2023a), centralized training (Local), and decentralized training (Global). For fair comparisons, we combine each federated learning strategy with different biomedical VLP methods. For baselines pre-trained in Local strategy, we report the averaged performance of the local models.

For fair comparisons, we re-implement the methods with the same backbones. To enable uni-modal self-supervised learning baselines to be applied to our setting, we employ the image-text contrastive loss with the same hyperparameters to our method for fairness. We utilize a ViT-base (Dosovitskiy et al., 2020) as our vision encoder and utilize the Bert-base (Devlin et al., 2018) as our text encoder. We preprocess the input following (Wang et al., 2022). We utilize an additional transformer layer from ViT-base and Bert-base as the align module for vision and language respectively.

## 5.2. Empirical Finding

In this section, we will demonstrate our key empirical findings for federated multi-modal pre-training under heterogeneous client datasets, which actually motivates us to propose our Federated distributional Robust Guidance-Based (FedRGB). We conduct experiments on the image-text retrieval task, which reflects the ability to capture vision-language alignments. We utilize the ConVIRT backbone strategy and consider the performance of the centralized pre-trained model (Global), the server model pre-trained in FedAvg (FedAvg), and the average performance of decen-

tralized pre-trained local models (Local.avg.).

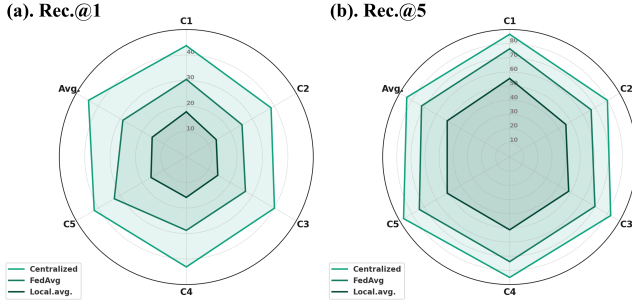


Figure 4. The comparison of retrieval acc. on each client denoted as  $\{C_i\}_{i=1}^5$ , of centralized, FedAvg, and averaged acc. of decentralized pre-trained models.

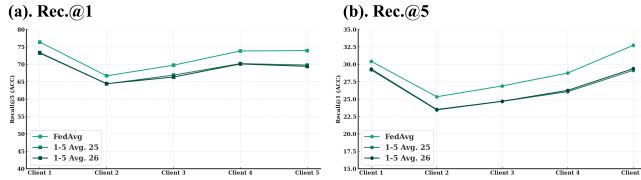


Figure 5. The performance of the server model after 25 com. turns and the averaged performance of corresponding client models after 25 and 26 com. turns, on each client denoted as  $\{Client_i\}_{i=1}^5$ .

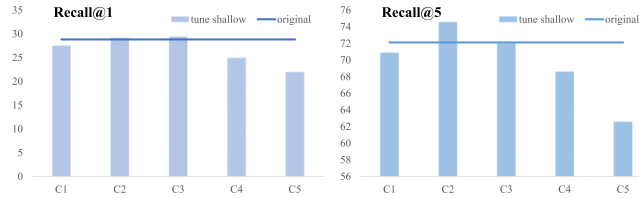


Figure 6. The averaged acc. on the test set of each client. We show the performance of FedAvg pre-trained baseline and its retrained models on different client datasets shown as  $\{C_i\}_{i=1}^5$ .

**FedAvg can aggregate semantics from local clients, but the performance would be damaged by data heterogeneity.** Figure 4 shows retrieval accuracies of the strategies we have considered, where the FedAvg pre-trained model achieves higher accuracies than those of decentralized ones with a large margin. However, the centralized pre-trained model acts as an upper bound and there still exists a great space for improvement for FedAvg. Table E in the appendix shows the detailed result. Further, we examine if updating the aggregated server model in FedAvg would result in distortion in the learned representation space.

**Retraining the server model on local datasets would distort its feature encoders.** Figure 5 demonstrates the effect of distortion by fitting local cross-modal alignments of the corresponding client datasets. We consider a set of models that finished the 25th local iteration and their corresponding aggregated server model. While the average accuracy of local models is less than their aggregated model, the average performance of models re-trained on local clients starting

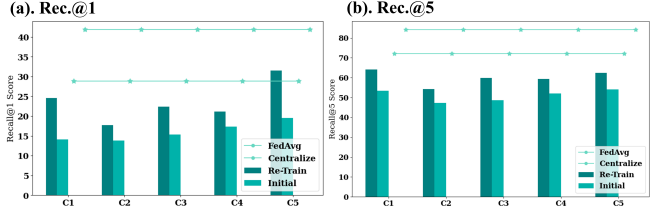


Figure 7. The averaged acc. on each client. We show the acc. of centralized and FedAvg pre-trained baselines, and de-centralized pre-trained models shown as  $\{C_i\}_{i=1}^5$  retrained on the union of training splits of client datasets.

from the aggregated model degrades a lot. Table E in the appendix shows the detailed results.

**Diverse information is aggregated in shallow layers that mainly extract feature semantics.** We re-train the first 4 shallow layers of the aggregated server model on local clients’ datasets for 500 iteration steps. As shown in figure 6, the performance of retrained models decreases a lot, which means shallow layers that extract feature semantics are distorted by heterogeneous local datasets. Table E in the appendix shows the detailed results.

**De-centralized pre-trained deep layers that act as the align module is harmful for extracting diverse semantics.** We re-train the first 4 shallow layers of the decentralized pre-trained model on the union of client datasets for 500 steps. Although the performance has successfully increased, there is still a large gap between that of the FedAvg pre-trained baselines and them as shown in Figure 7. Therefore, the frozen deep layers prevent the model from learning more diverse semantics from the scaled dataset. Table E in the appendix shows the detailed results.

Overall, from the empirical findings, we conclude that federated multimodal pre-training is sensitive to the data heterogeneity which results in learning distorted cross-modal alignment. Simply averaging the local model weights does not solve this issue essentially. Thus, we are motivated to propose our FedRGB.

### 5.3. Main Result

**Our method learns robust and enriched cross-modal alignment and has better transferability.** Table 5.2 shows the image-text retrieval results. Here we utilize the CONVIRT as the backbone pre-training method. We report the average recall accuracy and the worst-case recall accuracy. The two sets of acc. are higher than those of FedAvg, which means our model can not only capture more cross-modal alignment but optimize the performance on the worst client dataset, which verifies the robustness and fairness of our DRO-based strategy. Table 5.2 shows the results of the classification and segmentation downstream tasks. In general, our method has better transferability than the traditional FedAvg strategy, most of the compared metrics of our method

Table 2. Downstream task performance. We report the few-shot classification accuracy on Covid and RSNA, the retrieval accuracy on Chest imaGenome, and the Dice score on RSNA.

Strategy	RSNA (cls.)		Covid (cls.)		RSNA (seg.)		Chest imaG. (ret.)			
	1%	10%	1%	10%	1%	10%	Rec.@1	Rec.@5	Wst.@1	Wst.@5
Decentralized	82.27	82.83	79.45	88.25	67.44	70.75	15.51	51.12	13.62	45.97
FedX (Han et al., 2022)	80.16	81.17	80.50	89.25	71.27	71.61	3.22	16.76	1.58	11.94
FedMAE (Yan et al., 2023)	76.97	80.66	42.25	49.00	69.48	73.38	5.05	23.91	4.34	20.86
FedEMA (Zhuang et al., 2022)	82.81	83.19	79.25	86.50	70.94	73.65	24.01	67.05	21.85	62.44
FedAvg (Lu et al., 2023a)	83.19	83.31	78.00	88.50	69.59	71.50	28.83	72.12	25.34	66.68
FedRGB (Ours)	<b>83.21</b>	<b>83.54</b>	<b>82.50</b>	<b>90.00</b>	<b>71.51</b>	<b>74.08</b>	<b>29.49</b>	<b>73.03</b>	<b>26.99</b>	<b>67.65</b>
Centralized	83.39	84.61	82.50	92.00	72.60	76.35	41.45	84.22	38.55	79.98

Table 3. Downstream task performance on different multi-modal pre-training backbone methods.

Strategy	Method	RSNA (cls.)		Covid (cls.)		RSNA (seg.)		Chest imaG. (ret.)			
		1%	10%	1%	10%	1%	10%	Rec.@1	Rec.@5	Wst.@1	Wst.@5
Decentralized	GLoRIA	82.34	82.89	77.90	88.75	71.07	72.13	17.15	52.50	15.19	48.73
FedAvg	GLoRIA	83.16	83.28	77.50	89.00	71.37	72.38	29.90	73.80	27.78	69.46
FedRGB (Ours)	GLoRIA	<b>83.39</b>	<b>83.51</b>	<b>78.50</b>	<b>89.25</b>	<b>72.43</b>	<b>73.50</b>	<b>30.94</b>	<b>73.89</b>	<b>27.86</b>	<b>69.53</b>
Centralized	GLoRIA	84.01	84.74	82.25	91.75	73.63	73.64	41.69	84.04	39.00	80.52
Decentralized	MGCA	81.90	82.71	77.80	87.55	62.77	70.20	15.21	50.44	13.37	45.39
FedAvg	MGCA	82.63	83.54	75.75	88.25	70.06	71.39	29.33	73.71	26.81	<b>70.49</b>
FedRGB (Ours)	MGCA	<b>82.76</b>	<b>83.61</b>	<b>77.75</b>	<b>88.25</b>	<b>70.71</b>	<b>72.52</b>	<b>29.96</b>	<b>74.15</b>	<b>27.11</b>	69.53
Centralized	MGCA	83.96	84.49	79.50	89.50	70.71	72.52	39.89	83.50	36.88	80.28

are higher than those of the baseline, and are closer to those of the centralized pre-trained model, which is the upper bound baseline. Other self-supervised baselines that aim to tackle the data heterogeneity have weaker performance compared to FedAvg, we analyze that this is due to the lack of the modeling of heterogeneous multi-modal alignment.

**Previous single-modality methods cannot be adapted directly for multi-modal data.** Table 5.2 shows the performance of adapted self-supervised federated learning methods which focus on single-modality. From the results, we observe that our method beats these baselines by a large margin, which indicates that previous single-modality methods cannot be easily adapted directly for multi-modal data. Particularly, FedMAE and the FedX perform much worse than other federated learning strategies. We conjecture this is because both of them have ignored modeling the cross-modal alignment. Specifically, FedMAE’s masking strategies might hurt the alignment of image and text modalities, and FedX’s single-modality strategy can’t be adapted to model the image-text cross-modal interaction. Instead, we think FedAvg is still a strong baseline compared to other adapted methods, as we observed in the experiments. That’s because FedAvg doesn’t hurt the ability to learn cross-modal alignment of backbone pre-training models by adding augmented losses.

**Our method can be transferred to multiple multi-modal pre-training methods.** Table 5.2 shows the downstream

task performance of the MGCA and the GLoRIA backbone pre-training method when combined with our strategy. Our method has successfully upgraded MGCA and GLoRIA to adapt to the heterogeneous federated multi-modal pre-training scene, as shown in the significant improvement of the classification and segmentation downstream tasks.

5.4. Analysis experiment

In this section, we mainly conduct analysis experiments using the SLIA backbone method for pre-training unless specifically stated.

Table 4. Ablation results. We report the few-shot classification accuracy and the retrieval accuracy.

Strategy	1% (cls.)		Chest imaG. (ret.)			
	Covid	RSNA	Rec.@1	Rec.@5	Wst.@1	Wst.@5
→avg.alig.	83.14	79.75	28.31	72.18	26.26	66.56
→CL	82.91	78.25	28.81	71.03	25.95	66.42
ours	<b>83.21</b>	<b>80.50</b>	<b>29.49</b>	<b>26.99</b>	<b>73.03</b>	<b>67.65</b>

Table 5. Ablation experiment results on the zero-shot generalization ability of our method on the real-world dataset.

Strategy	O.O.D		In domain		In domain Wst.	
	Rec.@1	Rec.@5	Rec.@1	Rec.@5	Rec.@1	Rec.@5
FedX	12.31	61.04	3.22	16.76	1.58	11.94
FedMAE	12.93	63.72	5.05	23.91	4.34	20.86
FedEMA	15.19	66.94	24.01	67.05	21.85	62.44
FedAvg	15.3	66.62	28.83	72.12	25.34	66.68
FedRGB (Ours)	<b>15.43</b>	<b>67.29</b>	<b>29.49</b>	<b>73.03</b>	<b>26.99</b>	<b>67.65</b>



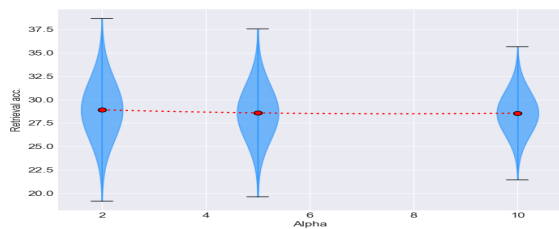


Figure 8. The trade-off adjusted by the hyper-parameter  $\alpha$ .

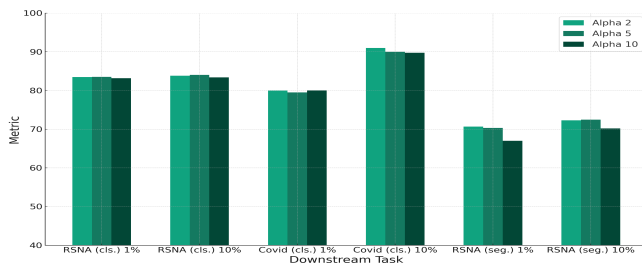


Figure 9. The role of the hyper-parameter  $\alpha$ .

**Robust teacher align module is better than simply averaged one.** To investigate the efficiency of the robust align module, we replace it with an align module that is simply averaged by local ones and pre-train a new model. As shown in table 5.4, the downstream performance of the replaced one is lower than the original one. This means the robust align module can enhance the ability to capture cross-modal alignments and learn transferable representation.

**Strong regularization is better than weak regularization for guiding the updation.** To investigate the effect of the guidance from the robust align module, we replace the L-2 regularization with contrastive loss as a weaker regularization and pre-train a new model. As shown in table 5.4, the weaker guidance leads to lower classification accuracy and retrieval accuracy in the downstream tasks.

**Guidance hyper-parameter adjusts the average and disparity of client performances.** Figure 8 shows that higher guidance achieves smaller disparity while bringing less harm on average performance. We changed the hyperparameter  $\alpha$  from 2 to 10, the disparity of the retrieval accuracy on test sets of different clients decreased significantly while there was only a slight loss on the averaged performance. On the other hand, Figure 9 shows that increasing  $\alpha$  wouldn't result in a penalty in the transferability of the pre-trained backbone, the downstream task performances are maintained at a high level as we enlarge the guidance. Detailed results can be seen in Table E.

**Convergence check:** The downstream performance of the pre-trained got promoted as we increased the number of comm. turns. After 20 communications, the performance turned out to be stable which verified the convergent ability of our method. Detailed results can be seen in Table E.

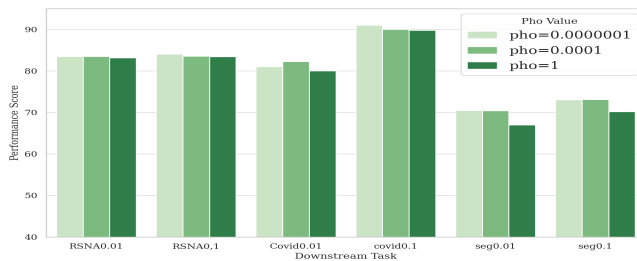


Figure 10. The role of the radius of the uncertainty set  $\rho$ .

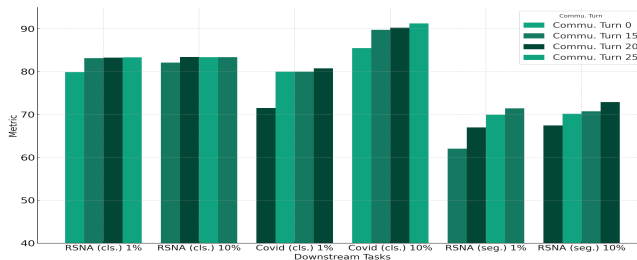


Figure 11. Robustness & convergence on the number of comm. turns.

### Our method has better classification accuracies on unseen out-of-distribution multi-modal X-Ray datasets.

The multi-modal retrieval accuracy in the unseen domain of our method beats the baseline by a large margin as shown in Table 5.4, which verifies our method's ability to learn generalizable cross-modal alignment. Meanwhile, our FedRGB has higher in-domain averaged and worst-case acc.. Therefore, improvements in the in-domain performance of FedRGB do not come at the cost of decreased out-of-domain performance.

**Smaller radius of uncertain set brings higher generalization and transferability on downstream task.** Figure 10 shows the downstream performance of models pre-trained with different radius of uncertainty set in the DRO process. As the  $\rho$  increases, the performance of fine-tuning-based downstream tasks shows an upward trend. Detailed results can be seen in Table D.

## 6. Conclusion

Data limitation is a long-standing problem in the multi-modal learning domain. Despite federated learning can leveraging datasets from multiple sources while guaranteeing privacy issues, its performance would be damaged by data heterogeneity. Inspired by our empirical findings on the impact of heterogeneity on federated multi-modal learning, we propose the FedRGB framework to mitigate heterogeneity for federated biomedical vision-language pre-training. The efficiency of our method has been verified by comprehensive experiments.

## 7. Limitation

The design of the proposed FedRGB approach has taken it into serious consideration to mitigate the potential negative societal impact.. For example, to tackle the data privacy issue, FedRGB has avoided the transmission of any data or latent representations during all server-client communications, while only transferring model parameters and loss, thereby minimizing the risk of privacy leakage in federated learning as much as possible. However, our model may still be subject to privacy-related issues due to the communication of model parameters, which is a common problem faced by other federated learning methods as well. There are also research studies in this line to avoid privacy leakage from model parameters.

For fairness, our method aims at optimizing the performance of the worst-case client to promote model equity across different cohorts, which has shown great generalizable ability on unseen data. This approach ensures that the pre-trained model not only performs well and fairly on the data from hospitals participating in the federated training but also demonstrates good performance on hospitals that did not participate in the training. Meanwhile we acknowledge that there may still exist limitations. Firstly, If we can resolve the trade-off between privacy protection and data representation communication, it may allow us to design more advanced algorithms to further enhance the performance of federated multimodal pre-training models.

Furthermore, in this work we mainly consider the multimodal medical datasets of X-Ray imageport due to the limitation of the public datasets. However, some rare diseases and more complicated modalities in various medical applications lack paired data, which] may bring other challenges for federated multimodal pretraining.

## 8. Acknowledgement

Zitao Shuai and Liyue Shen acknowledges support from U-M MIDAS PODS Grant and U-M MICDE Catalyst Grant, and computing resource support from NSF ACCESS Program. This work used NCSA Delta GPU through allocation CIS230133 and ELE230011 from the Advanced Cyberinfrastructure Coordination Ecosystem: Services & Support (ACCESS) program, which is supported by National Science Foundation grants 2138259, 2138286, 2138307, 2137603, and 2138296.

## References

Bae, S., Kyung, D., Ryu, J., Cho, E., Lee, G., Kweon, S., Oh, J., Ji, L., Chang, E. I., Kim, T., et al. Ehrxqa: A multi-modal question answering dataset for electronic health records with chest x-ray images. *arXiv preprint*

*arXiv:2310.18652*, 2023.

Bannur, S., Hyland, S., Liu, Q., Perez-Garcia, F., Ilse, M., Castro, D. C., Boecking, B., Sharma, H., Bouzid, K., Thieme, A., et al. Learning to exploit temporal structure for biomedical vision-language processing. In *Proceedings of the IEEE/CVF Conference on Computer Vision and Pattern Recognition*, pp. 15016–15027, 2023.

Bao, H., Wang, W., Dong, L., Liu, Q., Mohammed, O. K., Aggarwal, K., Som, S., Piao, S., and Wei, F. Vlmo: Unified vision-language pre-training with mixture-of-modality-experts. *Advances in Neural Information Processing Systems*, 35:32897–32912, 2022.

Bigolin Lanfredi, R., Zhang, M., Auffermann, W. F., Chan, J., Duong, P.-A. T., Srikumar, V., Drew, T., Schroeder, J. D., and Tasdizen, T. Reflax, a dataset of reports and eye-tracking data for localization of abnormalities in chest x-rays. *Scientific data*, 9(1):350, 2022.

Blei, D. M., Ng, A. Y., and Jordan, M. I. Latent dirichlet allocation. *Journal of machine Learning research*, 3(Jan): 993–1022, 2003.

Boecking, B., Usuyama, N., Bannur, S., Castro, D. C., Schwaighofer, A., Hyland, S., Wetscherek, M., Naumann, T., Nori, A., Alvarez-Valle, J., et al. Making the most of text semantics to improve biomedical vision–language processing. In *European conference on computer vision*, pp. 1–21. Springer, 2022.

Capitani, G., Bolelli, F., Porrello, A., Calderara, S., and Ficarra, E. Clusterfix: A cluster-based debiasing approach without protected-group supervision. In *Proceedings of the IEEE/CVF Winter Conference on Applications of Computer Vision*, pp. 4870–4879, 2024.

Chen, C., Feng, X., Zhou, J., Yin, J., and Zheng, X. Federated large language model: A position paper. *arXiv preprint arXiv:2307.08925*, 2023a.

Chen, H., Zhang, Y., Krompass, D., Gu, J., and Tresp, V. Feddat: An approach for foundation model finetuning in multi-modal heterogeneous federated learning. *arXiv preprint arXiv:2308.12305*, 2023b.

Chen, L., Gan, Z., Cheng, Y., Li, L., Carin, L., and Liu, J. Graph optimal transport for cross-domain alignment. In *International Conference on Machine Learning*, pp. 1542–1553. PMLR, 2020a.

Chen, T., Kornblith, S., Norouzi, M., and Hinton, G. A simple framework for contrastive learning of visual representations. In *International conference on machine learning*, pp. 1597–1607. PMLR, 2020b.

- Collins, L., Hassani, H., Mokhtari, A., and Shakkottai, S. Exploiting shared representations for personalized federated learning. In *International conference on machine learning*, pp. 2089–2099. PMLR, 2021.
- Cotter, A., Jiang, H., Gupta, M., Wang, S., Narayan, T., You, S., and Sridharan, K. Optimization with non-differentiable constraints with applications to fairness, recall, churn, and other goals. *Journal of Machine Learning Research*, 20(172):1–59, 2019.
- Deng, Y., Kamani, M. M., and Mahdavi, M. Distributionally robust federated averaging. *Advances in neural information processing systems*, 33:15111–15122, 2020.
- Devlin, J., Chang, M.-W., Lee, K., and Toutanova, K. Bert: Pre-training of deep bidirectional transformers for language understanding. *arXiv preprint arXiv:1810.04805*, 2018.
- Diao, E., Ding, J., and Tarokh, V. Heterofl: Computation and communication efficient federated learning for heterogeneous clients. *arXiv preprint arXiv:2010.01264*, 2020.
- Dosovitskiy, A., Beyer, L., Kolesnikov, A., Weissenborn, D., Zhai, X., Unterthiner, T., Dehghani, M., Minderer, M., Heigold, G., Gelly, S., et al. An image is worth 16x16 words: Transformers for image recognition at scale. *arXiv preprint arXiv:2010.11929*, 2020.
- Duchi, J., Shalev-Shwartz, S., Singer, Y., and Chandra, T. Efficient projections onto the  $l_1$ -ball for learning in high dimensions. In *Proceedings of the 25th international conference on Machine learning*, pp. 272–279, 2008.
- Duchi, J. C. and Namkoong, H. Learning models with uniform performance via distributionally robust optimization. *The Annals of Statistics*, 49(3):1378–1406, 2021.
- Ghosh, A., Hong, J., Yin, D., and Ramchandran, K. Robust federated learning in a heterogeneous environment. *arXiv preprint arXiv:1906.06629*, 2019.
- Han, P., Liu, Z., Liu, Z., and Xiong, C. Distributionally robust unsupervised dense retrieval training on web graphs. *arXiv preprint arXiv:2310.16605*, 2023.
- Han, S., Park, S., Wu, F., Kim, S., Wu, C., Xie, X., and Cha, M. Fedx: Unsupervised federated learning with cross knowledge distillation. In *European Conference on Computer Vision*, pp. 691–707. Springer, 2022.
- Hemker, K., Smidjievski, N., and Jamnik, M. Healnet-hybrid multi-modal fusion for heterogeneous biomedical data. *arXiv preprint arXiv:2311.09115*, 2023.
- Huang, S.-C., Shen, L., Lungren, M. P., and Yeung, S. Gloria: A multimodal global-local representation learning framework for label-efficient medical image recognition. In *Proceedings of the IEEE/CVF International Conference on Computer Vision*, pp. 3942–3951, 2021.
- Huang, W., Ye, M., and Du, B. Learn from others and be yourself in heterogeneous federated learning. In *Proceedings of the IEEE/CVF Conference on Computer Vision and Pattern Recognition*, pp. 10143–10153, 2022.
- Jiang, M., Wang, Z., and Dou, Q. Harmofl: Harmonizing local and global drifts in federated learning on heterogeneous medical images. In *Proceedings of the AAAI Conference on Artificial Intelligence*, volume 36, pp. 1087–1095, 2022.
- Kim, S., Lee, N., Lee, J., Hyun, D., and Park, C. Heterogeneous graph learning for multi-modal medical data analysis. In *Proceedings of the AAAI Conference on Artificial Intelligence*, volume 37, pp. 5141–5150, 2023.
- Krishnan, R., Rajpurkar, P., and Topol, E. J. Self-supervised learning in medicine and healthcare. *Nature Biomedical Engineering*, 6(12):1346–1352, 2022.
- Ladbury, C., Amini, A., Govindarajan, A., Mambetsariev, I., Raz, D. J., Massarelli, E., Williams, T., Rodin, A., and Salgia, R. Integration of artificial intelligence in lung cancer: Rise of the machine. *Cell Reports Medicine*, 2023.
- Li, D. and Wang, J. Fedmd: Heterogenous federated learning via model distillation. *arXiv preprint arXiv:1910.03581*, 2019.
- Li, D., Yang, Y., Song, Y.-Z., and Hospedales, T. Sequential learning for domain generalization. In *European Conference on Computer Vision*, pp. 603–619. Springer, 2020a.
- Li, J., Li, D., Xiong, C., and Hoi, S. Blip: Bootstrapping language-image pre-training for unified vision-language understanding and generation. In *International Conference on Machine Learning*, pp. 12888–12900. PMLR, 2022a.
- Li, Q., Diao, Y., Chen, Q., and He, B. Federated learning on non-iid data silos: An experimental study. In *2022 IEEE 38th International Conference on Data Engineering (ICDE)*, pp. 965–978. IEEE, 2022b.
- Li, T., Sahu, A. K., Talwalkar, A., and Smith, V. Federated learning: Challenges, methods, and future directions. *IEEE signal processing magazine*, 37(3):50–60, 2020b.
- Li, Y., Mao, H., Girshick, R., and He, K. Exploring plain vision transformer backbones for object detection. In *European Conference on Computer Vision*, pp. 280–296. Springer, 2022c.

- Liu, J., Shen, Z., Cui, P., Zhou, L., Kuang, K., and Li, B. Distributionally robust learning with stable adversarial training. *IEEE Transactions on Knowledge and Data Engineering*, 2022.
- Lu, S., Liu, Z., Liu, T., and Zhou, W. Scaling-up medical vision-and-language representation learning with federated learning. *Engineering Applications of Artificial Intelligence*, 126:107037, 2023a.
- Lu, W., Yu, H., Wang, J., Teney, D., Wang, H., Chen, Y., Yang, Q., Xie, X., and Ji, X. Zoopfl: Exploring black-box foundation models for personalized federated learning. *arXiv preprint arXiv:2310.05143*, 2023b.
- McMahan, B., Moore, E., Ramage, D., Hampson, S., and y Arcas, B. A. Communication-efficient learning of deep networks from decentralized data. In *Artificial intelligence and statistics*, pp. 1273–1282. PMLR, 2017.
- Moayeri, M., Pope, P., Balaji, Y., and Feizi, S. A comprehensive study of image classification model sensitivity to foregrounds, backgrounds, and visual attributes. In *Proceedings of the IEEE/CVF Conference on Computer Vision and Pattern Recognition*, pp. 19087–19097, 2022.
- Nguyen, H. Q., Lam, K., Le, L. T., Pham, H. H., Tran, D. Q., Nguyen, D. B., Le, D. D., Pham, C. M., Tong, H. T., Dinh, D. H., et al. Vindr-cxr: An open dataset of chest x-rays with radiologist’s annotations. *Scientific Data*, 9(1):429, 2022.
- Oquab, M., Darcet, T., Moutakanni, T., Vo, H., Szafraniec, M., Khalidov, V., Fernandez, P., Haziza, D., Massa, F., El-Nouby, A., et al. Dinov2: Learning robust visual features without supervision. *arXiv preprint arXiv:2304.07193*, 2023.
- Peng, C., Koniusz, P., Guo, K., Lovell, B. C., and Moghadam, P. Multivariate prototype representation for domain-generalized incremental learning. *arXiv preprint arXiv:2309.13563*, 2023.
- Petryk, S., Dunlap, L., Nasser, K., Gonzalez, J., Darrell, T., and Rohrbach, A. On guiding visual attention with language specification. In *Proceedings of the IEEE/CVF Conference on Computer Vision and Pattern Recognition*, pp. 18092–18102, 2022.
- Radford, A., Kim, J. W., Hallacy, C., Ramesh, A., Goh, G., Agarwal, S., Sastry, G., Askell, A., Mishkin, P., Clark, J., et al. Learning transferable visual models from natural language supervision. In *International conference on machine learning*, pp. 8748–8763. PMLR, 2021.
- Rieke, N., Hancox, J., Li, W., Milletari, F., Roth, H. R., Albarqouni, S., Bakas, S., Galtier, M. N., Landman, B. A., Maier-Hein, K., et al. The future of digital health with federated learning. *NPJ digital medicine*, 3(1):119, 2020.
- Saab, K., Hooper, S., Chen, M., Zhang, M., Rubin, D., and Ré, C. Reducing reliance on spurious features in medical image classification with spatial specificity. In *Machine Learning for Healthcare Conference*, pp. 760–784. PMLR, 2022.
- Sapkota, H., Ying, Y., Chen, F., and Yu, Q. Distributionally robust optimization for deep kernel multiple instance learning. In *International Conference on Artificial Intelligence and Statistics*, pp. 2188–2196. PMLR, 2021.
- Shih, G., Wu, C. C., Halabi, S. S., Kohli, M. D., Prevedello, L. M., Cook, T. S., Sharma, A., Amorosa, J. K., Arteaga, V., Galperin-Aizenberg, M., et al. Augmenting the national institutes of health chest radiograph dataset with expert annotations of possible pneumonia. *Radiology: Artificial Intelligence*, 1(1):e180041, 2019.
- Simon, C., Faraki, M., Tsai, Y.-H., Yu, X., Schultze, S., Suh, Y., Harandi, M., and Chandraker, M. On generalizing beyond domains in cross-domain continual learning. In *Proceedings of the IEEE/CVF Conference on Computer Vision and Pattern Recognition*, pp. 9265–9274, 2022.
- Su, S., Yang, M., Li, B., and Xue, X. Cross-domain federated adaptive prompt tuning for clip. *arXiv preprint arXiv:2211.07864*, 2022.
- Volpi, R., Larlus, D., and Rogez, G. Continual adaptation of visual representations via domain randomization and meta-learning. In *Proceedings of the IEEE/CVF Conference on Computer Vision and Pattern Recognition*, pp. 4443–4453, 2021.
- Wang, F., Zhou, Y., Wang, S., Vardhanabhuti, V., and Yu, L. Multi-granularity cross-modal alignment for generalized medical visual representation learning. *Advances in Neural Information Processing Systems*, 35:33536–33549, 2022.
- Wang, L., Lin, Z. Q., and Wong, A. Covid-net: A tailored deep convolutional neural network design for detection of covid-19 cases from chest x-ray images. *Scientific reports*, 10(1):19549, 2020.
- Wu, J. T., Agu, N. N., Lourentzou, I., Sharma, A., Paguio, J. A., Yao, J. S., Dee, E. C., Mitchell, W., Kashyap, S., Giovannini, A., et al. Chest imagenome dataset (version 1.0.0). *PhysioNet*, 5:18, 2021.
- Wu, S., Fu, X., Wu, F., and Zha, Z.-J. Cross-modal semantic alignment pre-training for vision-and-language navigation. In *Proceedings of the 30th ACM International Conference on Multimedia*, pp. 4233–4241, 2022.
- Yan, R., Qu, L., Wei, Q., Huang, S.-C., Shen, L., Rubin, D., Xing, L., and Zhou, Y. Label-efficient self-supervised



- federated learning for tackling data heterogeneity in medical imaging. *IEEE Transactions on Medical Imaging*, 2023.
- Yang, J., Duan, J., Tran, S., Xu, Y., Chanda, S., Chen, L., Zeng, B., Chilimbi, T., and Huang, J. Vision-language pre-training with triple contrastive learning. In *Proceedings of the IEEE/CVF Conference on Computer Vision and Pattern Recognition*, pp. 15671–15680, 2022.
- Yu, Q., Liu, Y., Wang, Y., Xu, K., and Liu, J. Multimodal federated learning via contrastive representation ensemble. *arXiv preprint arXiv:2302.08888*, 2023a.
- Yu, S., Muñoz, J. P., and Jannesari, A. Federated foundation models: Privacy-preserving and collaborative learning for large models. *arXiv preprint arXiv:2305.11414*, 2023b.
- Zhang, F., Kuang, K., Chen, L., You, Z., Shen, T., Xiao, J., Zhang, Y., Wu, C., Wu, F., Zhuang, Y., et al. Federated unsupervised representation learning. *Frontiers of Information Technology & Electronic Engineering*, 24(8): 1181–1193, 2023a.
- Zhang, F., Shuai, Z., Kuang, K., Wu, F., Zhuang, Y., and Xiao, J. Unified fair federated learning for digital healthcare. *Patterns*, 2023b.
- Zhang, G., Wei, S., Pang, H., and Zhao, Y. Heterogeneous feature fusion and cross-modal alignment for composed image retrieval. In *Proceedings of the 29th ACM International Conference on Multimedia*, pp. 5353–5362, 2021.
- Zhang, Y., Gao, H., Pei, J., and Huang, H. Robust self-supervised structural graph neural network for social network prediction. In *Proceedings of the ACM Web Conference 2022*, pp. 1352–1361, 2022a.
- Zhang, Y., Jiang, H., Miura, Y., Manning, C. D., and Langlotz, C. P. Contrastive learning of medical visual representations from paired images and text. In *Machine Learning for Healthcare Conference*, pp. 2–25. PMLR, 2022b.
- Zhou, K. and Wang, X. E. Fedvln: Privacy-preserving federated vision-and-language navigation. In *European Conference on Computer Vision*, pp. 682–699. Springer, 2022.
- Zhuang, W., Wen, Y., and Zhang, S. Divergence-aware federated self-supervised learning. *arXiv preprint arXiv:2204.04385*, 2022.
- Zhuang, W., Chen, C., and Lyu, L. When foundation model meets federated learning: Motivations, challenges, and future directions. *arXiv preprint arXiv:2306.15546*, 2023.

## A. Problem Formulation

We aim at mitigating the data heterogeneity issues in federally pre-training biomedical vision-language models to better capture the semantic alignment between the two modalities, with heterogeneous private datasets from different clients. In this section, we will formulate our problem setup, assumptions, and related notations.

**Federated Vision-Language Pre-training.** In this paper, we consider the federated vision-language pre-training (VLP) problem in the biomedical domain. Suppose we are given  $N$  clients  $\{C_i\}_{i=1}^N$ , each client has a corresponding local yet private dataset  $\{D_i\}_{i=1}^N$  that can't be easily shared due to privacy issues. Without access to centralized pre-training, federated pre-training aims to conduct vision-language representation learning across local clients, while still capture a robust and generalizable cross-modal alignment, by efficiently aggregating client models  $\{M_i\}_{i=1}^N$  trained on their private datasets.

Similar to conventional federated learning scenarios, our federated pre-training consists of multiple communication turns. For communication turn  $t$ , client models  $\{M_i\}_{i=1}^N$  completed the same number of local iteration steps respectively, and the server receives and aggregates the weights sent from local models to produce the aggregated server model  $M^t$ . Then it will be sent back to clients and re-trained on  $\{D_i\}_{i=1}^N$  separately to get new local models  $\{M_i^{t+1}\}_{i=1}^N$ .

The federated vision-language pre-training is a more practical and general task compared to related works. Table 3 lists the most similar settings in previous works, and the difference between our task and theirs.

**Data Formulation.** We consider the multimodal datasets including vision and language modalities  $X, Y$ , consisting of respective data samples  $X = \{x_i\}_{i=1}^n, Y = \{y_i\}_{i=1}^m, n, m \in N^+$ . We assume there exists latent variables  $U$  that embed semantics across two modalities such that  $X = T_x(U), Y = T_y(U)$ , where  $T_x(\cdot), T_y(\cdot)$  are assumed transformations that is not explicit to know. For example, the disease category of a given X-ray radiology-report pair is a latent variable connecting these two modalities, which determines the pathology region of the radiology image and semantics in the diagnosis report. Thus, we assume each client has paired image-text data that are implicitly correlated through the same latent variables. Therefore, local client datasets could be written as  $\mathcal{D} : \{D_i : (T_x(u), T_y(u)), u \sim P_i(U)\}_{i=1}^N$ . Here, we assume the local datasets are heterogeneous, which means the distribution of latent variables  $P_i(U)$  is different across clients.

We formulate two distributions  $\mu_i \in P(X_i), \nu_i \in P(Y_i)$  following (Chen et al., 2020a) as  $\mu_i = \sum_{j=1}^{n_i} a_j \delta_{T_x(u_j)}_{i,j}$  and  $\nu_i = \sum_{j=1}^{n_i} b_j \delta_{T_y(u_j)}_{i,j}$ , with  $\delta_x$  as the Dirac function centered on  $x$ . The weight vectors  $a_i = \{a_j\}_{j=1}^{n_i} \in \Delta_{n_i}$

and  $b_i = \{b_j\}_{j=1}^{n_i} \in \Delta_{n_i}$  belong to the  $(n - 1)$ -dim simplex, where  $\mu_i$  and  $\nu_i$  are probability distributions. This formulation can also be applied to feature vectors or representations. For a given set of distributions  $\{P_i\}_{i=1}^N$ , we can form a new distribution  $P^c = \sum_{i=1}^N w_i P_i$ ,  $\mathbf{w} \in \Delta$  where  $\Delta$  is a  $(N - 1)$ -dim simplex by weighted averaging the sample vectors.

**Model Architectures.** Following the VLP works (Radford et al., 2021; Yang et al., 2022), we frame the VLP using a dual-encoder structure, where the model for each modality consists of a feature encoder module  $f(\cdot)$  that outputs feature vectors given the raw input, and a feature alignment module  $g(\cdot)$  that projects feature vectors to aligned representations in the shared embedding space. Denote the feature vector as  $s$ , and the aligned representation as  $z$ . We model the outputs of the encoder and alignment modules as conditional distributions. Specifically, the encoder takes the multi-modal raw input to generate semantic embeddings of the corresponding modality, which could be formulated as  $P(s|U)$ . Similarly, that of the alignment module can be formulated as  $P(z|S, U)$ .

## B. Details of Learning Unbiased Cross-modal Alignment via Distribution-based Optimization

In order to guide the local client training, we need to provide a teacher alignment module as mentioned in the last section, which can capture globally unbiased and generalizable cross-domain alignment. How can we obtain such a teacher guidance model? We propose to learn the unbiased cross-domain alignment by considering the robustness across various distributions of local clients.

A teacher alignment module should avoid distorting the aggregated feature encoder while learning the cross-modal alignments. Additionally, we introduce a much harder task to force the module to be more robust to biased alignment, by considering the influence of the biased alignment module on the feature encoder. Furthermore, to learn a teacher model that performs well on varies data distributions, we minimize distortion degree under the most biased local alignment with the ‘‘worst-case’’ local data distribution.

Inspired by the distributionally robust optimization (DRO) (Cotter et al., 2019), we model the de-centralized pre-training framework as a two-stage DRO learning process. In the first stage, the local models are trained with  $\mathcal{L}_{local}$  (Eq. 2), while the whole model is jointly optimized with the guidance of the teacher alignment module. In the second stage, we learn a robust teacher alignment module that performs well conditioned on the worst-case local models where the feature encoder is distorted the most severely.

We aim to optimize the alignment module on the worst-case distribution of an uncertainty set constructed by the local aligner and local data distribution, which represents possible cases that the model would encounter. We construct the uncertainty set based on the distribution of client datasets and local aligners learned in the first stage. From the probabilistic view, the local aligners could be written as  $P(z|U, f)$ , which takes the output of the given encoder  $f$  to generate the aligned representations, while  $f$  takes the raw input from the local data distribution  $P(U)$  to generate the semantic embedding that has not well learned the cross-modal alignment. Therefore, the distribution to be considered should be  $P(z, U|f)$ . Hence the uncertainty set can be written as:

$$Q^c : \{D(Q||P^c) \leq \rho\}, P^c = \sum_{i=1}^N w_i P_i(z, U|f), w \in \Delta_{N-1} \quad (7)$$

where  $N$  is the number of clients,  $\Delta$  is a  $(N - 1)$ -dim simplex,  $D$  is a discrepancy measure, and  $\rho$  is the uncertainty radius that measures the uncertainty degree of the unseen distributions and influences model’s generalization ability.

Finally, with the teacher align module denoted as  $g^*$ , indicating the aggregated encoder after the first stage training, the learning object in the second stage can be formulated as:

$$\min_{g^*} \max_{P \in Q^c} \mathcal{L}_{dro}(g^*, P, f^*) \quad (8)$$

Following (Zhang et al., 2023b), the optimization goal can be constructed by distributions  $P_i$  of the support set:

$$\min_{g^*} \max_{\mathbf{w} \in \Delta_{N-1}} \sum_{i=1}^N w_i \mathcal{L}_{dro}(g^*, P_i, f), s.t. D(N\mathbf{w}||\mathbf{1}) \leq \rho \quad (9)$$

where  $\mathcal{L}_{dro}(g^*, P_i, f^*)$  are the losses calculated on the local clients respectively. While we learn  $g^*$  by gradient descent, the mirror gradient descent process of optimizing  $\mathbf{w}$  could be solved efficiently (Zhang et al., 2023b; Duchi et al., 2008):

$$w_i = \text{Proj}_{\mathcal{Q}_c} \left( w_i e^{\gamma v_i} / \sum_{i=1}^N w_i e^{\gamma v_i}, \rho \right) \quad (10)$$

where  $\text{Proj}_{\mathcal{Q}_c}$  refers to the projection to  $\{w : D(N\mathbf{w}||\mathbf{1}) \leq \rho\}$ ,  $v_i$  represents the loss  $\mathcal{L}_{dro}(g^*, P_i, f^*)$ .

We alternatively optimize the  $\mathbf{w}$  and the teacher align module. For each communication turn of the federated learning, we first obtain an averaged encoder, and a set of local align modules in the first stage. Then we solve the weights and optimize the parameters of the teacher align module. Hence the  $\mathbf{w}$  could be written in a more trackable form as:

$$w_i^{(r+1)} = \text{Proj}_{\mathcal{Q}_c} \left( w_i^{(r)} e^{\gamma v_i^{(r)}} / \sum_{i=1}^N w_i^{(r)} e^{\gamma v_i^{(r)}}, \rho \right) \quad (11)$$

where  $r$  refers to the communication turn..

Finally, we formulate  $\mathcal{L}_{dro}$  to measure the performance of the teacher align module of alleviating distortion on the encoder. Based on equations (3) and (4), we update the teacher alignment module in local clients with weights  $\mathbf{w}$ . Specifically, given a client  $c$ , we use  $f^*$  learned in the first stage of the current communication turn to generate features  $(\tilde{v}^c, \tilde{l}^c)$ , and a learnable copy of  $f^*$  to generate distorted features  $(v^c, l^c)$ . The distorted features are input to the frozen  $g$  to calculate the task loss  $L_{task}$ , and are input to the  $g^*$  to get calibrated representations  $(z_I^{c*}, z_T^{c*})$ . Meanwhile,  $(\tilde{v}^c, \tilde{l}^c)$  are input to  $g^*$  to get representation  $(z_I^{c*}, z_T^{c*})$  for regularization. The regularization term could be written as:

$$\mathcal{L}_{dro,\tau} = \beta \left( \sum_{i=1}^{N_c} (z_{I,i}^{c*} - z_{I,i}^{c*})^2 + \sum_{i=1}^{N_c} (z_{T,i}^{c*} - z_{T,i}^{c*})^2 \right) + \mathcal{L}_{CL,\tau} \quad (12)$$

where  $\mathcal{L}_{CL}$  is the contrastive loss (Radford et al., 2021) between  $(z_{img,i}^{fz,c*}, z_{txt,i}^{fz,c*})_{i=0}^{N_c}$ , and  $N_c$  refers to the number of samples in the client  $c$ .

## C. Experiment Details

### C.1. Pre-training setup

Following (Wang et al., 2022) we utilize the MIMIC-CXR (Bigolin Lanfredi et al., 2022) dataset for multi-modal pre-training. This dataset is widely used in the biomedical multi-modal learning domain, with 227, 835 image-text pairs from 65, 379 patients. Some related works also have imported additional features to image-text pairs to augment the data. However, we only use the image-text pairs for pre-training to make the results more generalizable.

During the pre-training, local clients only have access to their highly heterogeneous datasets. To construct the heterogeneous client datasets, following (Yan et al., 2023) we employ the Latent Dirichlet Allocation (LDA) (Blei et al., 2003) to divide the MIMIC-CXR dataset into 5 partitions based on a selected sensitive attribute. For implementation, we import the corresponding attribute information of given image-text pairs from the Chest-Imagenone dataset (Wu et al., 2021) and divide local datasets based on disease category. The disease category is a multi-label binary attribute and is transformed into a multi-class label. That’s because the words in the clinical report are highly related to the disease category as illustrated in 12. We set the heterogeneity degree in the LDA algorithm to be 1 and the subgroups of the MIMIC-CXR that are used as local datasets are summarized in Table C.1.

Specifically, we select 5 commonly considered diseases (Bannur et al., 2023): ‘Edema’, ‘Pleural Effusion’, ‘Consolidation’, ‘Pneumothorax’, and ‘Pneumonia’. We set the non-NaN value to 1 and then set NaN value to 0 to con-

struct a 5-way binary multi-label. Then we get 2<sup>5</sup>-category multi-class label, and we run LDA on it. The distribution of the disease of the client dataset is summarized in Table C.1.

Table 6. Distortion of local training of FedAvg method. We show the performance gap between the server and local retrained models. We employ the decrease in the similarity of the image embedding and text embedding to be an indicator of distortion.

FedAvg	Test on C1	Test on C2	Test on C3	Test on C4	Test on C5
Retrain On C1	0.092	0.078	0.08	0.073	0.082
Retrain On C2	0.054	0.049	0.046	0.047	0.048
Retrain On C3	0.069	0.072	0.07	0.066	0.067
Retrain On C4	0.092	0.09	0.084	0.093	0.088
Retrain On C5	0.073	0.08	0.07	0.068	0.087
Avg	0.076	0.0738	0.07	0.0694	0.0744

We divide the MIMIC-CXR into 5 heterogeneous subgroups to construct 5 client datasets. Each divided dataset consists of train splits and validation splits based on the notation of the MIMIC-CXR. We use  $4 \times A40$  for pre-training and set the batch size to 388. We set the learning rate to  $2 \times 10^{-5}$ , the number of communications to 25. We set the updating step size  $\gamma = 1$ , and uncertainty radius  $\rho = 1$ , hyperparameter  $\alpha = 1, \beta = 2$  in the main experiments. For each communication, we randomly sample 50 batches of data from the client datasets. To obtain the guidance, we run an extra communication for our method.

### C.2. Downstream tasks

We conduct Few-shot classification, Medical image segmentation, and Image Retrieval downstream tasks to evaluate the generalization ability of the pre-trained model.

**Few-shot classification.** To verify the efficiency of the pre-trained model on the general medical image task, we test their performance on multiple image classification benchmarks: (1) RSNA Pneumonia Detection (RSNA) (Shih et al., 2019), the task is to predict if the image reflects a pneumonia-positive phenomenon. (2) Covidx (Wang et al., 2020), which has three categories that COVID-19, non-COVID pneumonia and normal. We fine-tune our pre-trained model with an additional linear layer on 1%, 10% percentage of the training dataset of downstream tasks, and evaluate the image classification accuracy. For evaluation, we report the classification accuracy of the models on them.

**Medical image segmentation.** To investigate the transfer ability of our model on fine-grained tasks, we conduct experiments on medical image segmentation on the RSNA (Wang et al., 2020) benchmark. We follow (Wang et al., 2022) to convert object detection ground truths of RSNA into masks for semantic segmentation. Similar to (Huang et al., 2021), we construct a U-Net framework using a decoder and our pre-trained image encoder. During the fine-tuning, we freeze the encoder and fine-tune the decoder using 1%, 10%

**Report Sample 1:**

Previous mild pulmonary edema and possible concurrent pneumonia has all cleared. Heart is top-normal size, improved, and pleural effusions have resolved. Right hilar vessels are still enlarged, perhaps due to pulmonary arterial hypertension. Lateral view shows atherosclerotic coronary calcification in the left circumflex.

**Label:**

**Edema**

**Pneumonia**

**Pleural Effusions**

**Report Sample 2:**

Allowing for differences in technique and projection, there has been little interval change in the appearance of the chest since the previous radiograph, with no new focal areas of consolidation to suggest the presence of pneumonia. Multifocal linear areas of scarring appear unchanged, previously attributed to sarcoidosis. Band-like opacity at periphery of left lung base has slightly worsened and is attributed to localized atelectasis.

**Label:**

**Pneumonia**

Figure 12. Illustration of the divided heterogeneous subgroups for each client.

of the training data of the downstream dataset, and then use the Dice score to evaluate the performance of our model.

**Image retrieval.** To verify if the pre-trained models have learned the semantics and alignment relationships between the image and text contained in the pre-training dataset, we conduct the image retrieval downstream task. Specifically, we utilize the validation splits of the local clients to test the image retrieval performance of the aggregated models. For a text from a given batch of input image-text pairs, we calculate the similarities between this text and images in this batch. Then we sort these similarities and select the top-1 and top-5 images from them. If the corresponding image of the text is contained in the selected set, then the image is retrieved correctly. Here we utilize the top-1 recall accuracy and top-5 recall accuracy to evaluate the pre-trained models.

**Out-of-Distribution testing benchmark.** We adapt the EHRXQA (Bae et al., 2023) VQA dataset for evaluation. This dataset is built on the meta-data notation of MIMIC-CXR (Bigolin Lanfredi et al., 2022) and ChestImaGenome (Wu et al., 2021). We merge the question and answer sentences as the text input and use the corresponding image to construct the image-text pairs for the multi-modal retrieval task. Other settings are the same as the ordinary image retrieval task.

**C.3. Backbones and Baselines**

We focus on upgrading biomedical vision-language pre-training (VLP) strategies to heterogeneous federated learning scenes. Since federated heterogeneous VLP is a new topic, we adopt existing biomedical VLP baselines to federated strategies (Lu et al., 2023a). Specifically, we consider adopting simple language-image contrastive alignment (ConVIRT) (Zhang et al., 2022b; Radford et al., 2021), global-local language-image contrastive alignment (GLoRIA) (Huang et al., 2021), and Multi-Granularity Cross-modal Alignment (MGCA) (Wang et al., 2022). For federated learning strategies, we consider simple averaging (FedAvg) (McMahan et al., 2017; Lu et al., 2023a), centralized training (Local), and decentralized training (Global).

For fair comparisons, we combine each federated learning strategy with different biomedical VLP methods. For baselines pre-trained in Local strategy, we report the averaged performance of the local models.

For fair comparisons, we implement the method with the same backbones as our method. We utilize a ViT-Base model as our vision encoder and utilize the Bert-Base as our text encoder. We pre-process the input image following (Wang et al., 2022) to resize the radiology graph to the size of  $224 \times 224$  to match the vision encoder.

**D. Additional Analysis Experiment**

We report the communication costs and training costs of our method and other FL methods on both the server and client sides in Table 9. As shown in the table, the additional computational overhead introduced by our method is within an acceptable range.

**Our method has successfully avoided the distortion caused by heterogeneous datasets during the local training.** Empirically, we demonstrate the effectiveness of this guidance-based local training strategy. Specifically, we retrain the model on each local dataset with the same backbone methods and setting and conduct the study on the change of similarity between embeddings of paired image and text. We show the performance gap between the server and local retrained models. The reduced similarity of the image embedding and text embedding from paired data can be regarded as an indicator of "distortion" of cross-modal alignment. As reported in Table 6 and Table 11, we observe that the average decrease on the similarity of image and text embedding of our method is much smaller compared to FedAvg baseline.

**Role of the number of clients that participated in the federated pre-training.** We have conducted experiments on how the number of clients participating in the federated pre-training affects the performance of the learned model. As shown in the Table E, we have observed that bringing more diverse clients for the federated pre-training is likely



Table 7. The distribution of the sensitive attribute age-decile. From this table, we can verify that the local datasets are highly heterogeneous.

Edema	P. E.	Consolid.	Pneumothorax	Pneumonia	C1	C2	C3	C4	C5
					8251	52931	23153	16054	2983
Yes					367	130	4362	1993	2671
	Yes				67	11425	5825	778	655
Yes	Yes				945	1693	3472	2640	1607
		Yes			1641	261	599	791	1057
Yes		Yes			420	61	198	245	14
	Yes	Yes			253	50	18	805	913
Yes	Yes	Yes			434	95	27	303	153
			Yes		476	2504	128	8791	1097
Yes			Yes		827	284	559	603	156
	Yes		Yes		4366	1866	3507	2815	1140
Yes	Yes		Yes		5965	217	510	109	921
		Yes	Yes		123	80	444	111	84
Yes		Yes	Yes		48	9	101	4	269
	Yes	Yes	Yes		807	121	3	922	670
Yes	Yes	Yes	Yes		723	818	42	246	69
				Yes	7447	3656	1505	246	1395
Yes				Yes	278	927	719	1547	453
	Yes			Yes	98	970	1111	639	1145
Yes	Yes			Yes	2777	3019	2276	105	466
		Yes		Yes	10	323	120	227	760
Yes		Yes		Yes	31	57	153	28	9
	Yes	Yes		Yes	30	16	238	148	91
Yes	Yes	Yes		Yes	92	a74	9	101	36
			Yes	Yes	208	286	48	15	33
Yes			Yes	Yes	70	214	248	1	90
	Yes		Yes	Yes	164	76	39	126	872
Yes	Yes		Yes	Yes	133	251	417	155	1224
		Yes	Yes	Yes	71	6	15	8	8
Yes		Yes	Yes	Yes	2	56	42	3	20
	Yes	Yes	Yes	Yes	156	18	11	44	279
Yes	Yes	Yes	Yes	Yes	38	156	201	38	183

Table 8. Descriptive Statistics of the subgroups.

Disease	C1	C2	C3	C4	C5
Edema	13150	8061	13336	8121	8341
P.E.	17048	20865	17706	9974	10424
Consolid.	4879	2201	2221	4024	4615
Pneumoth.	14177	6962	6315	13991	7115
Pneumonia	11605	10105	7152	3431	7064

Table 9. Summarization of computation costs.

Method	Train Params	Train time	Server Cost	Info. Trans.
De-centralized	172.6 M	14.62s/fit	863M FLOP	172.6 M
FedAvg	172.6 M	14.62s/fit	863M FLOP	172.6 M
FedMAE	226.1M	14.95s/fit	1130.5M FLOP	226.1M
FedX	172.6 M	22.66s/fit	863M FLOP	172.6 M
FedEMA	172.6 M	14.59s/fit	863M FLOP	172.6 M
Ours [1st stage]	190.4M	15.4s/fit	951.2M FLOP	190.4M
Ours [2nd stage]	190.4M	23.68s/fit	89M FLOP	17.8M
Centralized	172.6 M	14.62s/fit	863M FLOP	172.6 M

to improve the performance of the pre-trained model.

### E. Detailed Experiment Results

Here we show the detailed experiment results.

Table 10. Detailed results on the analysis experiments of the role of hyper-parameter  $\alpha$ .

$\rho$	RSNA (cls.)		Covid (cls.)		RSNA (seg.)	
	1%	10%	1%	10%	1%	10%
$\rho = 1e - 7$	83.51	84.04	81.00	91.00	70.44	73.05
$\rho = 1e - 4$	83.51	83.54	82.25	90.00	70.39	73.11
$\rho = 1$	83.16	83.41	80.00	89.75	66.98	70.18

Table 11. Distortion of local training of ours method. We show the performance gap between the server and local retrained models. We employ the decrease in the similarity of the image embedding and text embedding to be an indicator of distortion.

Ours	Test on C1	Test on C2	Test on C3	Test on C4	Test on C5
Retrain On C1	0.025	0.023	0.017	0.034	0.01
Retrain On C2	0.046	0.05	0.043	0.057	0.063
Retrain On C3	0.05	0.052	0.044	0.055	0.036
Retrain On C4	0.062	0.043	0.038	0.041	0.033
Retrain On C5	0.071	0.058	0.048	0.066	0.053
Avg	<b>0.0508</b>	<b>0.0452</b>	<b>0.038</b>	<b>0.0506</b>	<b>0.039</b>

Table 12. The comparison of retrieval acc. on each client denoted as  $\{C_i\}_{i=1}^5$ , of centralized, FedAvg, and averaged acc. of decentralized pre-trained models using the ConVIRT backbone. We report the local models of decentralized pre-training strategy as Decentralized<sub>*i*</sub>.

Strategy	Recall@1 (ACC)					Recall@5 (ACC)						
	C1	C2	C3	C4	C5	Avg.	C1	C2	C3	C4	C5	Avg.
Centralized	43.65	38.55	40.08	43.10	41.86	44.45	86.63	79.98	82.65	84.99	86.83	84.22
FedAvg	30.43	25.34	26.90	28.75	32.73	28.83	76.39	66.68	69.75	73.84	73.94	72.12
Decentralized <sub>1</sub>	17.68	14.71	15.37	18.18	14.14	16.01	56.99	49.56	51.29	54.55	55.10	53.50
Decentralized <sub>2</sub>	15.33	11.62	13.85	14.96	13.83	13.92	54.84	41.93	46.20	47.90	45.62	47.30
Decentralized <sub>3</sub>	17.41	13.08	14.12	15.07	15.39	15.01	50.40	44.21	46.37	49.72	52.53	48.65
Decentralized <sub>4</sub>	16.54	14.34	14.08	15.36	17.35	15.53	57.02	45.72	47.45	52.38	57.63	52.04
Decentralized <sub>5</sub>	21.68	14.34	14.20	15.56	19.50	17.06	57.89	48.43	50.18	52.36	61.66	54.10
Local.avg.	17.73	13.62	14.32	15.83	16.04	15.51	55.43	45.97	48.30	51.38	51.12	51.12

Table 13. The performance of the server model after 25 commu. turns and the averaged performance of corresponding local models after 25 and 26 commu. turns, on each client denoted as  $\{C_i\}_{i=1}^5$ . We utilize the ConVIRT as the backbone. We report the models after local update on client datasets of FedAvg pre-training strategy as Local<sub>*i*</sub>.

Strategy	com. turn	Recall@1 (ACC)					Recall@5 (ACC)				
		C1	C2	C3	C4	C5	C1	C2	C3	C4	C5
FedAvg	25	30.43	25.34	26.90	28.75	32.73	76.39	66.68	69.75	73.84	73.94
Local <sub>0</sub>	25	31.75	23.37	25.96	26.21	33.71	73.44	64.14	67.15	71.38	71.79
Local <sub>1</sub>	25	27.72	22.52	23.77	25.06	27.70	73.45	63.08	64.57	69.15	68.58
Local <sub>2</sub>	25	28.55	24.37	24.30	27.26	28.93	73.26	64.94	67.52	70.28	71.75
Local <sub>3</sub>	25	30.63	22.62	23.90	25.36	26.42	72.57	64.02	66.26	68.92	67.62
Local <sub>4</sub>	25	27.31	24.37	25.47	26.47	28.93	73.26	65.83	68.95	71.23	69.21
1-5 Avg.	25	29.19↓	23.45↓	24.68↓	26.07↓	29.14↓	73.20↓	64.40↓	66.89↓	70.20↓	69.79↓
Local <sub>0</sub>	26	29.91	23.18	25.24	26.66	33.05	73.44	64.14	67.15	71.38	71.79
Local <sub>1</sub>	26	28.7	23.05	23.95	25.91	27.37	74.48	63.37	64.12	69.69	67.93
Local <sub>2</sub>	26	30.9	23.85	25.42	27.67	29.89	72.40	65.57	67.42	71.56	71.12
Local <sub>3</sub>	26	30.11	22.66	23.41	24.45	27.05	73.09	63.48	65.32	67.48	67.31
Local <sub>4</sub>	26	26.96	24.81	25.47	26.6	29.55	73.61	66.03	69.17	71.19	69.54
1-5 Avg.	26	29.32↓	23.51↓	24.70↓	26.26↓	29.38↓	73.33↓	64.44↓	66.34↓	70.10↓	69.41↓

Table 14. Robustness check on communication turns.

Com.	RSNA (cls.)		Covid (cls.)		RSNA (seg.)		Chest imaG. (ret.)			
	1%	10%	1%	10%	1%	10%	Rec.@1	Rec.@5	Wst.@1	Wst.@5
commu.=0	79.89	82.11	71.50	85.50	62.03	67.46	3.27	16.44	2.53	13.54
commu.=15	83.16	83.41	80.00	89.75	66.98	70.18	28.56	71.83	2595	67.21
commu.=20	83.26	83.39	80.00	90.25	69.93	70.76	29.69	72.09	26.75	67.52
commu.=25	83.34	83.39	80.75	91.25	71.42	72.89	29.80	72.59	27.48	68.64

Table 15. Detailed results on the analysis experiments of the role of hyper-parameter  $\alpha$ .

Hyper. Alpha	RSNA (cls.)		Covid (cls.)		RSNA (seg.)		Chest imaG. (ret.)		
	1%	10%	1%	10%	1%	10%	Recall Acc.	Worst Acc.	Disparity
$\alpha = 2$	83.49	83.83	79.99	91.00	70.67	72.27	3.25	28.91	25.95
$\alpha = 5$	83.51	84.01	79.50	90.00	70.31	72.44	2.99	28.58	26.12
$\alpha = 10$	83.16	83.41	80.00	89.75	66.98	70.18	2.37	28.56	26.17

Table 16. Detailed results on the analysis experiments of the effect of the number of participated clients.

Num. Client	RSNA (cls.)		Covid (cls.)		RSNA (seg.)		Chest imaG. (ret.)			
	1%	10%	1%	10%	1%	10%	Rec@1 Acc.	Wst@1 Acc.	Rec@5 Acc.	Wst@5 Acc.
n=2	82.11	83.06	77.25	88.5	62.73	71.17	22.27	62.2	18.7	56.23
n=5	83.21	83.54	80.5	90	71.51	74.08	29.49	73.03	26.99	67.65

Table 17. The accuracy of the test set of each client. We show the performance of FedAvg pre-trained baseline and its retrained models on different client datasets. We report the models after local update on client datasets of FedAvg pre-training strategy as Local<sub>i</sub>.

position	model	com.	Recall@1 (ACC)						Recall@5 (ACC)					
			C0	C1	C2	C3	C4	Avg.	C0	C1	C2	C3	C4	Avg.
-	server	25	30.43	25.34	26.90	28.75	32.73	28.83	76.39	66.68	69.75	73.84	73.94	72.12
-	server	50	32.29	26.03	26.99	27.06	30.23	28.52↓	77.60	67.86	69.43	72.06	71.74	71.74↓
→ shallow	Local <sub>0</sub>	25	30.35	24.95	25.32	28.44	28.62	27.54↓	73.78	67.22	68.44	71.95	73.01	70.88↓
→ shallow	Local <sub>1</sub>	25	34.25	26.4	27.27	29.66	30.20	29.44↑	78.30	69.75	72.33	75.07	77.42	74.57↑
→ shallow	Local <sub>2</sub>	25	33.68	26.39	27.27	29.66	30.20	29.44↑	77.25	67.37	70.67	74.21	70.51	72.02↑
→ shallow	Local <sub>3</sub>	25	27.65	18.94	19.30	25.61	24.87	24.95↓	72.40	64.19	64.82	70.47	71.13	68.60↓
→ shallow	Local <sub>4</sub>	25	26.19	18.94	19.30	22.74	22.66	21.97↓	69.27	56.76	58.94	63.35	64.50	62.56↓

Table 18. The accuracy of the model on each client. We show the acc. of centralized and FedAvg pre-trained baselines and de-centralized pre-trained models shown as Local<sub>i</sub> retrained on the union of training splits of client datasets. We fine-tune shallow layers of the de-centralized pre-trained model with the union dataset.

strategy	model	Recall@1 (ACC)						Recall@5 (ACC)					
		C1	C2	C3	C4	C5	Avg.	C1	C2	C3	C4	C5	Avg.
Global	server	43.65	38.55	40.08	43.10	41.86	41.45	86.63	79.98	82.65	84.99	86.83	84.22
FedAvg	server	30.43	25.34	26.90	28.75	32.73	28.83	76.39	66.68	69.75	73.84	73.94	72.12
Decentralized	Local <sub>1</sub>	28.72	22.61	23.52	22.32	24.59	24.35	70.94	60.77	63.31	62.40	63.42	64.17
Decentralized	Local <sub>2</sub>	17.36	19.85	18.23	17.58	17.68	18.14	52.70	56.05	55.14	54.01	53.54	54.29
Decentralized	Local <sub>3</sub>	20.92	20.67	25.96	21.04	22.34	22.19	58.93	58.05	65.34	58.21	58.99	59.90
Decentralized	Local <sub>4</sub>	20.86	20.07	20.69	25.57	21.12	21.66	59.11	56.88	57.82	64.70	58.69	59.44
Decentralized	Local <sub>5</sub>	21.79	19.54	21.98	20.90	31.54	23.15	60.73	56.99	59.80	60.17	74.07	62.35
Decentralized	Local <sub>1</sub>	17.68	14.71	15.37	18.18	14.14	16.02	56.99	49.56	51.29	54.55	55.10	53.50
Decentralized	Local <sub>2</sub>	15.33	11.62	13.85	14.96	13.83	13.92	54.84	41.93	46.20	47.90	45.62	47.30
Decentralized	Local <sub>3</sub>	17.41	13.08	14.12	15.07	15.39	15.01	50.40	44.21	46.37	49.72	52.53	48.65
Decentralized	Local <sub>4</sub>	16.54	14.34	14.08	15.36	17.35	15.53	57.02	45.72	47.45	52.38	57.63	52.04
Decentralized	Local <sub>5</sub>	21.68	14.34	14.20	15.56	19.50	17.06	57.89	48.43	50.18	52.36	61.66	54.10

Table 19. Detailed ablation results.

Strategy	Recall@1 (ACC)						Recall@5 (ACC)					
	C1	C2	C3	C4	C5	Avg.	C1	C2	C3	C4	C5	Avg.
→avg.align.	30.11	26.26	26.63	30.30	28.27	28.31	74.65	66.56	70.23	73.62	75.83	72.18
→CL	30.80	25.95	26.27	29.24	31.78	28.81	74.13	66.42	68.09	71.65	74.86	71.03
ours	32.53	26.99	27.70	29.09	31.12	29.62	77.08	67.65	70.32	73.96	76.12	73.14